Postdecay quantum entanglement in top pair production

J. A. Aguilar-Saavedra
Instituto de Física Teórica IFT-UAM/CSIC, c/Nicolás Cabrera 13–15, 28049 Madrid, Spain

(Received 20 July 2023; accepted 3 October 2023; published 31 October 2023)

Top pairs produced at the Large Hadron Collider exhibit quantum entanglement of their spins near threshold and for boosted, central $t\bar{t}$ pairs. The entanglement is maintained between the decay products, in particular, between the top quark and the W^- boson from the antiquark (or vice versa, between $\bar{t}$ and W^+) in certain kinematical regions. Therefore, $t\bar{t}$ production provides a rare opportunity to verify the spin entanglement between a fermion and a boson. The tW entanglement can be probed at the 7σ level near threshold with run 2 data and at the 5σ level in the boosted region with the foreseen run 3 luminosity. In addition, the entanglement between the two W bosons can be probed at the 4σ level at the LHC run 3.

DOI: 10.1103/PhysRevD.108.076025

I. INTRODUCTION

Quantum mechanics is one of the fundamental pillars of modern particle physics and, as such, testing it thoroughly is of the utmost importance. Quantum entanglement can be tested at the energy frontier in pp collisions at the Large Hadron Collider (LHC). Proposals have been made for $t\bar{t}$ production [1–7], and a preliminary measurement has been performed by the ATLAS Collaboration [8]. Entanglement can be also tested for vector bosons from Higgs decays [9–11] and electroweak diboson production [12–14]. In all these cases, and other proposals for future colliders [15] the entanglement takes place between the spins of the produced particles, which are either fermion pairs ($t\bar{t}$, $\tau^+\tau^-$) or boson pairs (WW, ZZ, WZ). Top pair production also offers the rare and exciting possibility to test the spin entanglement between a fermion and a boson, namely, the top quark and the W^- from the $\bar{t}$ decay (or their charge conjugate). Previous tests of fermion-boson entanglement have been provided in Ref. [16], where electron-photon entangled pairs have been achieved by creating photons off an electron beam. Moreover, it allows one to test the "post-decay" entanglement: the coherence of the top pair is propagated to its decay products and can be observed in certain kinematical regions, and so it manifests that the decay of a particle is not a measurement in the quantum-mechanical sense.

In order to understand how the tW entanglement arises let us, for example, consider $t\bar{t}$ production from gluon fusion near threshold. The spin state is approximately a singlet

$$\psi_{t\bar{t}} = \frac{1}{\sqrt{2}}\left[\left|\tfrac{1}{2}\quad -\tfrac{1}{2}\right\rangle - \left|-\tfrac{1}{2}\quad \tfrac{1}{2}\right\rangle\right], \tag{1}$$

where we take the $\hat{z}$ spin quantization axis in the direction of one proton, $\hat{z} = \hat{p}_p \equiv (0,0,1)$ for definiteness. In general, the coherence between the t and W^- spins is lost upon integration over the $\bar{t}$ decay phase space and sum over $\bar{b}$ polarizations which are difficult, if not impossible, to measure. However, let us assume that the W^- three-momentum direction $\vec{p}_W$ in the $\bar{t}$ rest frame is close to the $\hat{z}$ axis (and therefore the $\bar{b}$ three-momentum approximately in the $-\hat{z}$ direction). The left-handed tbW interaction mediating the top quark decay produces a left chirality $\bar{b}$; therefore, up to small m_b/m_t effects, the $\bar{b}$ quark has positive helicity, i.e., it is in a $S_z = -\frac{1}{2}$ state. For a $S_z = -\frac{1}{2}$ top antiquark, this implies $S_z = 0$ for the W^- boson, because orbital angular momentum in the direction of motion vanishes. Conversely, for a $S_z = \frac{1}{2}$ top antiquark, it implies $S_z = +1$ for the W^-. Thus, the spin state of the tW pair is

$$\psi_{tW^-} = \frac{1}{\sqrt{a^2+b^2}}\left[a\left|\tfrac{1}{2}\quad 0\right\rangle - b\left|-\tfrac{1}{2}\quad 1\right\rangle\right], \tag{2}$$

where a and b are not expected to be equal because of polarization effects in the $\bar{t}$ decay: the W^- angular distribution in the $\bar{t}$ rest frame is not isotropic. If, instead, we consider $\vec{p}_W$ in the $-\hat{z}$ direction, the spin state is

$$\psi'_{tW^-} = \frac{1}{\sqrt{a^2+b^2}}\left[b\left|\tfrac{1}{2}\quad -1\right\rangle - a\left|-\tfrac{1}{2}\quad 0\right\rangle\right]. \tag{3}$$

In practice, it is sufficient to consider some relatively wide interval for the angle θ_W between $\vec{p}_W$ and either the positive or negative $\hat{z}$ axis to experimentally verify the entanglement.

II. THEORETICAL SETUP

For a system composed of two subsystems A and B, a mixed state is said to be separable if the density operator describing this state can be written in the form

$$\rho = \sum_n p_n \rho_n^A \otimes \rho_n^B, \tag{4}$$

where $\rho_n^{A,B}$ are density operators for the two subsystems A, B, respectively, and p_n are classical probabilities, $p_n \geq 0$ with $\sum_n p_n = 1$. If ρ cannot be written in this fashion, the state is said to be entangled. A necessary condition for the state to be separable is given by the Peres-Horodecki criterion [17,18]: taking the transpose of the density operator in one of the two subspaces, e.g., in the B space, the resulting density operator ρ^{T_2} must still be valid, in particular, with non-negative eigenvalues. This condition can be understood since, if ρ is expressed as in (4), the transpose of $(\rho_n^B)^T$ is still a valid density operator for B, therefore ρ^{T_2} is a valid density operator with non-negative eigenvalues. The Peres-Horodecki criterion is also a sufficient condition when the dimensions of the Hilbert spaces are $\dim \mathcal{H}_A = \dim \mathcal{H}_B = 2$, or $\dim \mathcal{H}_A = 2$, $\dim \mathcal{H}_B = 3$. We therefore use as an "entanglement indicator" the lowest eigenvalue of ρ^{T_2},

$$\lambda_1 \equiv \min\{\lambda_i\}. \tag{5}$$

When $\lambda_1 < 0$, this is a sufficient condition for entanglement. However, we point out that, even when all λ_i are positive, statistical fluctuations may result in negative eigenvalues when measuring ρ^{T_2} in data. The bias associated with this effect is discussed and corrected for, in Sec. IV.

We parametrize the top quark and W boson density matrices using irreducible tensor operators. For the top quark we use

$$t_1^1 = -\frac{1}{\sqrt{2}}(\sigma_1 + i\sigma_2), \quad t_{-1}^1 = \frac{1}{\sqrt{2}}(\sigma_1 - i\sigma_2), \quad t_0^1 = \sigma_3, \tag{6}$$

with σ_i the Pauli matrices. For the W boson we use an analogous definition for the $L = 1$ operators but with different normalization,

$$T_1^1 = -\frac{\sqrt{3}}{2}(S_1 + iS_2), \qquad T_{-1}^1 = \frac{\sqrt{3}}{2}(S_1 - iS_2),$$
$$T_0^1 = \sqrt{\frac{3}{2}} S_3, \tag{7}$$

with S_i the spin-1 operators in the Cartesian basis. The $L = 2$ operators are [19]

$$T_{\pm 2}^2 = \frac{2}{\sqrt{3}}(T_{\pm 1}^1)^2, \qquad T_{\pm 1}^2 = \sqrt{\frac{2}{3}}[T_{\pm 1}^1 T_0^1 + T_0^1 T_{\pm 1}^1],$$
$$T_0^2 = \frac{\sqrt{2}}{3}[T_1^1 T_{-1}^1 + T_{-1}^1 T_1^1 + 2(T_0^1)^2]. \tag{8}$$

The operators satisfy $(t_m^1)^\dagger = (-1)^m t_{-m}^1$, $(T_M^L)^\dagger = (-1)^M T_{-M}^L$, and their normalizations are chosen so that $\mathrm{tr}[t_{m_1}^1 (t_{m_2}^1)^\dagger] = 2\delta_{m_1 m_2}$, $\mathrm{tr}[T_{M_1}^{L_1} (T_{M_2}^{L_2})^\dagger] = 3\delta_{L_1 L_2}\delta_{M_1 M_2}$. The density operator of the tW pair can then be parametrized as

$$\rho_{tW} = \frac{1}{6}[\mathbb{1}_2 \otimes \mathbb{1}_3 + a_m t_m^1 \otimes \mathbb{1}_3 + A_{LM}\mathbb{1}_2 \otimes T_M^L + C_{mLM} t_m^1 \otimes T_M^L], \tag{9}$$

where a sum over repeated indices m, L, M is understood. The constants a_m and A_{LM} are the top and W boson polarizations, respectively, and C_{mLM} are their spin correlations. These coefficients satisfy

$$a_{-m} = (-1)^m a_m^*, \qquad A_{L-M} = (-1)^M A_{LM}^*,$$
$$C_{-mL-M} = (-1)^{m+M} C_{mLM}^*. \tag{10}$$

Therefore, a_0, A_{L0}, and C_{0L0} are real and the remaining coefficients are, in general, complex. We note that many previous studies for top polarization use a parametrization in terms of Pauli matrices and a real polarization vector P^{CAR} in Cartesian coordinates, with

$$P_1^{\mathrm{CAR}} = \frac{1}{\sqrt{2}}(-a_1 + a_{-1}), \qquad P_2^{\mathrm{CAR}} = -\frac{i}{\sqrt{2}}(a_1 + a_{-1}),$$
$$P_3^{\mathrm{CAR}} = a_3. \tag{11}$$

We prefer to use a polar basis with a complex polarization vector a_m, so that the treatment of the top quark and W boson is more alike. The explicit expressions of ρ_{tW} and $\rho_{tW}^{T_2}$ are given in the Appendix.

The different terms in the density operators are not directly accessible, but can be measured via the angular distributions of the top and W decay products, which are used as "spin analyzers." In our case, it is best to use the charged leptons $\ell = e, \mu$ from the $t \to W^+ b \to \ell^+ \nu b$ and $W^- \to \ell^- \nu$ decays, so for simplicity we particularize the otherwise general framework to this specific case. Let us label the three-momentum direction of ℓ^+ in the top quark rest frame as $\hat{p}_1$ and the three-momentum direction of ℓ^- in the W^- rest frame as $\hat{p}_2^*$. (The asterisk highlights the fact that the ℓ^- three-momentum is taken in the W rest frame.) In polar coordinates,

$$\hat{p}_1 = (\sin\theta_1\cos\varphi_1, \sin\theta_1\sin\varphi_1, \cos\theta_1),$$
$$\hat{p}_2^* = (\sin\theta_2^*\cos\varphi_2^*, \sin\theta_2^*\sin\varphi_2^*, \cos\theta_2^*). \quad (12)$$

The $(\hat{x}, \hat{y}, \hat{z})$ reference system, whose orientation is necessary to define the angles $\Omega_1 = (\theta_1, \varphi_1)$ and $\Omega_2^* = (\theta_2^*, \varphi_2^*)$, is the same one used to write the density operator. The charged lepton momenta in the t and W^- frames have to be obtained with a succession of boosts; see, for example, Ref. [20] for a detailed discussion.

The decay distributions can be obtained by convoluting the density operator with the appropriate decay angular density matrices [21]. For the top quark, the decay density matrix is

$$\Gamma_1 = \frac{1}{2}\begin{pmatrix} 1+\alpha\cos\theta_1 & \alpha\sin\theta_1 e^{i\varphi_1} \\ \alpha\sin\theta_1 e^{-i\varphi_1} & 1-\alpha\cos\theta_1 \end{pmatrix}, \quad (13)$$

with $\alpha = 1$ for the positive charged lepton. The W-decay density matrix is

$$\Gamma_2 = \frac{1}{4}\begin{pmatrix} 1+\cos^2\theta_2^* - 2\eta_\ell\cos\theta_2^* & \frac{1}{\sqrt{2}}(\sin 2\theta_2^* - 2\eta_\ell\sin\theta_2^*)e^{i\varphi_2^*} & (1-\cos^2\theta_2^*)e^{i2\varphi_2^*} \\ \frac{1}{\sqrt{2}}(\sin 2\theta_2^* - 2\eta_\ell\sin\theta_2^*)e^{-i\varphi_2^*} & 2\sin^2\theta_2^* & -\frac{1}{\sqrt{2}}(\sin 2\theta_2^* + 2\eta_\ell\sin\theta_2^*)e^{i\varphi_2^*} \\ (1-\cos^2\theta_2^*)e^{-i2\varphi_2^*} & -\frac{1}{\sqrt{2}}(\sin 2\theta_2^* + 2\eta_\ell\sin\theta_2^*)e^{-i\varphi_2^*} & 1+\cos^2\theta_2^* - 2\eta_\ell\cos\theta_2^* \end{pmatrix}, \quad (14)$$

with $\eta_\ell = 1$. The quadruple differential distribution can be obtained as

$$\frac{1}{\sigma}\frac{d\sigma}{d\Omega_1 d\Omega_2^*} = \frac{6}{(4\pi)^2}\sum_{i,j,r,s}(\rho_{tW})_{ir,js}(\Gamma_1)_{ij}(\Gamma_2)_{rs}, \quad (15)$$

with the indices $i, j = 1, 2$ corresponding to the top spin space and $r, s = 1, 2, 3$ to the W spin space. The algebra yields

$$\frac{1}{\sigma}\frac{d\sigma}{d\Omega_1 d\Omega_2^*} = \frac{1}{(4\pi)^2}[1 + a_m b_1 Y_1^m(\Omega_1) + A_{LM}B_L Y_L^M(\Omega_2^*) + C_{mLM}b_1 B_L Y_1^m(\Omega_1)Y_L^M(\Omega_2^*)], \quad (16)$$

with Y_L^M the spherical harmonics and

$$b_1 = \alpha\sqrt{\frac{4\pi}{3}}, \qquad B_1 = -\sqrt{2\pi}\eta_\ell, \qquad B_2 = \sqrt{\frac{2\pi}{5}}. \quad (17)$$

For $\bar{t}W^+$ entanglement, the same equations can be used, with $\alpha = -1$ for the negative charged lepton from the $\bar{t}$ decay and $\eta_\ell = -1$ for the positive lepton from W^+ decay.

The density operator for a vector boson pair using the parametrization of irreducible operators has been written before [10]. In our case,

$$\rho_{WW} = \frac{1}{9}[\mathbb{1}_3\otimes\mathbb{1}_3 + A_{LM}^1 T_M^L\otimes\mathbb{1}_3 + A_{LM}^2\mathbb{1}_3\otimes T_M^L + C_{L_1M_1L_2M_2}T_{M_1}^{L_1}\otimes T_{M_2}^{L_2}], \quad (18)$$

where the superscripts 1,2 refer to the W^+ and W^- boson, respectively. The corresponding angular distribution is

$$\frac{1}{\sigma}\frac{d\sigma}{d\Omega_1^* d\Omega_2^*} = \frac{1}{(4\pi)^2}[1 + A_{LM}^1 B_L^1 Y_L^M(\Omega_1^*) + A_{LM}^2 B_L^2 Y_L^M(\Omega_2^*) + C_{L_1M_1L_2M_2}B_{L_1}^1 B_{L_2}^2 Y_{L_1}^{M_1}(\Omega_1^*)Y_{L_2}^{M_2}(\Omega_2^*)], \quad (19)$$

where in this case the ℓ^+ three-momentum

$$\hat{p}_1^* = (\sin\theta_1^*\cos\varphi_1^*, \sin\theta_1^*\sin\varphi_1^*, \cos\theta_1^*) \quad (20)$$

is taken in the W^+ rest frame.

III. CALCULATIONAL SETUP

The $t\bar{t} \to \ell^+\nu b\ell^-\nu\bar{b}$ Monte Carlo samples required for our study are generated with MadGraph [22] at the leading order, using NNPDF 3.1 [23] parton density functions and setting as factorization and renormalization scale the average transverse mass, $Q = 1/2[(m_t^2 + p_{Tt}^2)^{1/2} + (m_{\bar{t}}^2 + p_{T\bar{t}}^2)^{1/2}]$, with p_T the transverse momentum in the usual notation. This is sufficient for our purpose, since next-to-leading order (NLO) corrections to the $t\bar{t}$ spin correlation coefficients are small [24]; the effect of including NLO corrections in entanglement studies has been explicitly tested in Ref. [3] and found to be small compared to the statistical uncertainty. NLO corrections to the top quark decay have a negligible effect in the charged lepton distributions, changing the value of α at the per-mille level [25]. The total cross section is normalized to the next-to-next-to-leading order prediction [26].

Two samples are generated, using a center-of-mass (c.m.) energy of 13 TeV. A first sample with $t\bar{t}$ invariant mass $m_{t\bar{t}} \leq 400$ GeV, containing 2.5×10^7 events, is used to test tW and WW entanglement near threshold. A second sample with 5×10^6 events is used to study tW entanglement in the boosted central region. This sample is generated with $m_{t\bar{t}} \geq 750$ GeV and also with a cut on the scattering

angle θ_t between the top quark momentum in the c.m. frame and $\hat{p}_p = (0,0,1)$, $|\cos\theta_t| \leq 0.7$.

We work at the parton level and do not include backgrounds, which are small for the $t\bar{t}$ dilepton decay channel, especially when the two leptons have different flavors. It is known that for the dilepton decay channel the final state can be reconstructed and the detector effects can be properly accounted for by an unfolding to parton level, as it has already been done by the ATLAS and CMS Collaborations for the measurement of $t\bar{t}$ spin correlation coefficients [27,28], using various methods for the reconstruction of the neutrino momenta via kinematic fitting [29,30]. Having this in mind, we use the true top quark and W boson momenta for the computations. We include an efficiency factor of 0.12 to take into account the detection and reconstruction efficiencies, i.e., that the final state objects are well identified and the reconstructed momenta have good agreement with the expected $t\bar{t}$ kinematics. This value is the average efficiency found in Ref. [3] with a fast detector simulation, which is smaller than the efficiency of 0.17 obtained in Ref. [31], also with fast simulation.

The reconstruction and unfolding also introduces a systematic uncertainty in the extracted quantities. The measurement performed by the ATLAS Collaboration [8] shows a significant modeling uncertainty when converting the particle-level measurement to the parton level near the threshold region, in particular, for the $t\bar{t}$ invariant mass bin used $340 \leq m_{t\bar{t}} \leq 380$ GeV. As pointed out in Ref. [5], the suppression of the $q\bar{q}$ component with a kinematical cut on the $t\bar{t}$ velocity in the laboratory frame[1] allows us to loosen the upper cut on $m_{t\bar{t}}$ while keeping the $t\bar{t}$ entanglement, and this might constitute an experimental advantage (at the tree level, raising the upper cut to $m_{t\bar{t}} \leq 390$ GeV increases the cross section by a factor 1.4). In our sensitivity estimations we include a bulk 10% systematic uncertainty in our entanglement indicator, namely, the lowest eigenvalue of ρ^{T_2}, to illustrate the effect of systematic uncertainties arising from reconstruction and unfolding. This figure may be too optimistic for a near-threshold measurement and, in any case, a detector-level study is necessary to precisely quantify the systematic uncertainty.

We use two different bases to measure polarizations and spin correlation coefficients. The beamline basis is defined with fixed vectors

$$\hat{x} = (1,0,0), \qquad \hat{y} = (0,1,0), \qquad \hat{z} = (0,0,1). \tag{21}$$

The helicity basis is defined with $\hat{z} = \hat{k}$, $\hat{x} = \hat{r}$, $\hat{y} = \hat{n}$, the K, R, and N axes being defined as follows:

(i) K axis (helicity): $\hat{k}$ is a normalized vector in the direction of the top quark three-momentum in the $t\bar{t}$ rest frame.

(ii) R axis: $\hat{r}$ is in the production plane and defined as $\hat{r} = (\hat{p}_p - \cos\theta_t \hat{k})/\sin\theta_t$.

(iii) N axis: $\hat{n} = \hat{k} \times \hat{r}$ is orthogonal to the production plane.

An alternative definition of the helicity basis can be implemented by introducing sign-flipping factors $\mathrm{sign}\cos\theta_t$ in the definition of the R and N axes [33]. With this sign flip, small values appear for a_1 and A_{11}, at the percent level, which have little effect on the value of the entanglement indicator λ_1.

Using either of these bases, the angles entering Eqs. (16) and (19) can be defined, and the coefficients can be measured by integration using an appropriate kernel, e.g., for the tW density operator,

$$\begin{aligned}
\int \frac{1}{\sigma}\frac{d\sigma}{d\Omega_1 d\Omega_2^*} Y_1^m(\Omega_1) d\Omega_1 d\Omega_2^* &= \frac{b_1}{4\pi} a_m, \\
\int \frac{1}{\sigma}\frac{d\sigma}{d\Omega_1 d\Omega_2^*} Y_L^M(\Omega_2^*) d\Omega_1 d\Omega_2^* &= \frac{B_L}{4\pi} A_{LM}, \\
\int \frac{1}{\sigma}\frac{d\sigma}{d\Omega_1 d\Omega_2^*} Y_1^m(\Omega_1) Y_L^M(\Omega_2^*) d\Omega_1 d\Omega_2^* &= \frac{b_1 B_L}{(4\pi)^2} C_{mLM}.
\end{aligned} \tag{22}$$

We remark that these equations are valid even if a kinematical selection is placed on the angle θ_W between $\vec{p}_W$ and the $\hat{z}$ direction, as discussed in the Introduction.[2] We can illustrate those arguments numerically, considering $gg \to t\bar{t}$ with $m_{tt} \leq 370$ GeV and using the beamline basis. In the basis of $\mathcal{H}_A \otimes \mathcal{H}_B$,

$$\left\{ \left|\tfrac{1}{2}\ \tfrac{1}{2}\right\rangle, \quad \left|\tfrac{1}{2}\ -\tfrac{1}{2}\right\rangle, \quad \left|-\tfrac{1}{2}\ \tfrac{1}{2}\right\rangle, \quad \left|-\tfrac{1}{2}\ -\tfrac{1}{2}\right\rangle \right\}, \tag{23}$$

the $t\bar{t}$ density matrix is, setting to zero entries at the 10^{-3} level or below,

$$\rho_{t\bar{t}} = \begin{pmatrix} 0.061 & 0 & 0 & 0 \\ 0 & 0.438 & -0.402 & 0 \\ 0 & -0.402 & 0.438 & 0 \\ 0 & 0 & 0 & 0.062 \end{pmatrix}. \tag{24}$$

This matrix has an eigenvector

$$\psi_{t\bar{t}} = \frac{1}{\sqrt{2}}\left[\left|\tfrac{1}{2}\ -\tfrac{1}{2}\right\rangle - \left|-\tfrac{1}{2}\ \tfrac{1}{2}\right\rangle \right], \tag{25}$$

with eigenvalue 0.84. That is, the $t\bar{t}$ pair is nearly produced in a spin-zero singlet, as it is expected close to threshold.

[1] Such variable has already been used by the ATLAS Collaboration in the $t\bar{t}$ charge asymmetry measurement [32].

[2] On the other hand, the negative lepton cannot be used as spin analyzer for $\bar{t}$ precisely due to this angular cut.

Placing a cut $\cos\theta_W \geq 0.9$, the tW^- density matrix is (see the Appendix for notation)

$$\rho_{tW^-} = \begin{pmatrix} 0.055 & 0 & 0 & 0 & 0 & 0 \\ 0 & 0.543 & 0 & -0.358 & 0 & 0 \\ 0 & 0 & 0.040 & 0 & 0 & 0 \\ 0 & -0.358 & 0 & 0.284 & 0 & 0 \\ 0 & 0 & 0 & 0 & 0.070 & 0 \\ 0 & 0 & 0 & 0 & 0 & 0.008 \end{pmatrix}. \tag{26}$$

This matrix has an eigenvector

$$\psi_{tW^-} = 0.818\left|\tfrac{1}{2} \quad 0\right\rangle - 0.574\left|-\tfrac{1}{2} \quad 1\right\rangle, \tag{27}$$

with eigenvalue 0.79, in full agreement with Eq. (2).

IV. SENSITIVITY ESTIMATES

We do not attempt a multidimensional optimization of the sensitivity to tW^- and W^+W^- entanglement. Instead, we select either of the regions previously used in Ref. [5] to study the $t\bar{t}$ entanglement,

$$\begin{aligned} &\text{Threshold:}\ m_{t\bar{t}} \leq 390\ \text{GeV}, && \beta \leq 0.9, \\ &\text{Boosted:}\ m_{t\bar{t}} \geq 800\ \text{GeV}, && |\cos\theta_t| \leq 0.6, \end{aligned} \tag{28}$$

with

$$\beta = \left|\frac{p_t^z + p_{\bar{t}}^z}{E_t + E_{\bar{t}}}\right| \tag{29}$$

being the velocity of the $t\bar{t}$ pair in the laboratory frame, in obvious notation. We add to these constraints a cut on $\cos\theta_W$, specified below. Each of these regions, defined by a selection on $m_{t\bar{t}}$, β or $\cos\theta_t$, and $\cos\theta_W$, in which the tW^- and W^+W^- entanglement is measured, will be referred to as the "measurement region."

The selection of the smallest eigenvalue of ρ^{T_2} as entanglement indicator entails a bias, because when reconstructing ρ^{T_2} from a finite sample, a negative eigenvalue may arise even for a positive-definite ρ^{T_2}, due to statistical fluctuations that cause mismeasurements of the coefficients in the angular distribution. Therefore, the sensitivity to experimentally establish the entanglement is assessed by comparing (i) pseudodata corresponding to the standard model (SM) prediction, in a measurement region where there is entanglement, and (ii) the separability hypothesis. Pseudoexperiments are performed to obtain numerically the probability density function (PDF) of two quantities:

(i) the smallest eigenvalue of ρ^{T_2} in the measurement region, which we label as λ_1^{e};

(ii) the smallest eigenvalue λ_1^{s} of the positive-definite operator ρ in a suitable "calibration region," where the smallest eigenvalue of ρ is nearly zero.

The former, when $\lambda_1^{\mathrm{e}} < 0$, corresponds to the entanglement scenario. The latter is a proxy for the separability hypothesis. The reader may wonder why we do not use for the separability hypothesis the smallest eigenvalue of ρ^{T_2} in a quite different kinematical region such that the state is separable. We believe it is preferable from the experimental point of view to use a calibration region that is as kinematically as close as possible, in $m_{t\bar{t}}$, β, and $\cos\theta_t$, to the measurement region. On the other hand, dropping the constraint on $\cos\theta_W$ does not always result in a separable state.

From a large pool of $t\bar{t} \to \ell^+\nu b\ell^-\nu\bar{b}$ events in the measurement region, we select a random sample of N events corresponding to the cross section times the assumed luminosity, including the 0.12 efficiency factor previously mentioned. For each sample we calculate the values of the coefficients in the angular distribution, cf. (16) or (19), and subsequently we obtain the matrix expression of ρ^{T_2}. This matrix is diagonalized numerically and the lowest eigenvalue λ_1^{e} is obtained. Repeating this procedure n times, we obtain a PDF for λ_1^{e}, which is Gaussian to an excellent approximation.

Subsequently, we identify a calibration region with $\vec{p}_W$ very close to the $\hat{z}$ axis, in which the density operator ρ has the lowest eigenvalue λ_1^{s} quite close to zero, typically at the level of few per mille. The rest of eigenvalues happen to be similar to those of ρ^{T_2}. We perform n pseudoexperiments, selecting a random sample of N events in this calibration region, calculating the values of the coefficients in the angular distribution, obtaining the matrix expression of ρ and calculating its lowest eigenvalue λ_1^{s}. With this second set of pseudoexperiments we obtain the PDF of λ_1^{s} for the positive definite operator ρ, which has a bias toward negative values due to statistical fluctuations. This PDF is very well approximated by a skew-normal distribution. We remark that it is essential that the same number N of events per sample is used to calculate the PDFs of λ_1^{e} and λ_1^{s} so that the latter gives an estimation of the bias toward negative values in the former. Clearly, the bias is smaller the larger the statistics, and in some of the examples below it turns out to be unimportant.

A. tW^- entanglement near threshold

For this analysis we select the beamline basis for simplicity, as the helicity basis gives quite the same results. The reason for these bases being equivalent is that the spin-singlet state is rotationally invariant, so the $t\bar{t}$ spin configuration is the same in either basis. The measurement region is defined as

$$m_{t\bar{t}} \leq 390\ \text{GeV}, \qquad \beta \leq 0.9, \qquad \cos\theta_W \geq 0.3. \tag{30}$$

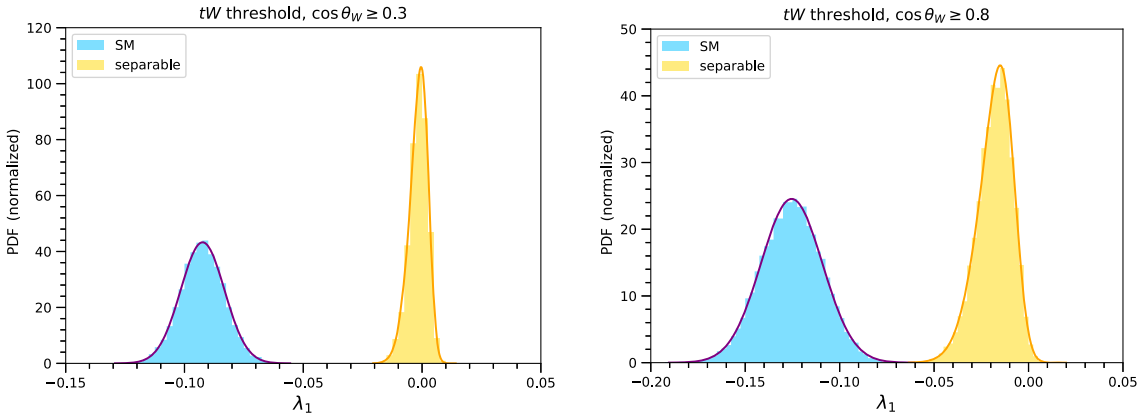

FIG. 1. Probability density functions of (i) λ_1^e in the threshold measurement region (blue), used to determine tW^- entanglement in the SM; and (ii) λ_1^s in its calibration region (yellow), used as a proxy of the lowest eigenvalue for a separable state.

The cross section with these cuts is 1.8 pb. We assume a luminosity of 139 fb^{-1}, as collected in run 2 of the LHC. With this luminosity, the number of expected events is $N = 30140$, with the assumed reconstruction efficiency. The calibration region is defined with $\cos\theta_W \geq 0.98$.

The PDFs of λ_1^e and λ_1^s obtained for $N = 30140$ events with $n = 10^4$ pseudoexperiments are presented in the left panel of Fig. 1. In order to better understand the bias issue, we show in the right panel the same for $\cos\theta_W \geq 0.8$, in which case $N = 8870$. The comparison of the two examples shows a couple illuminating features:

(1) A tighter cut on $\cos\theta_W$ lowers the mean of the distribution $\mu_{\lambda_1^e}$—which we identify with the "measured" value λ_1^e to simplify the notation—but increases the standard deviation $\sigma_{\lambda_1^e}$, which we identify with the statistical uncertainty on λ_1^e. Namely, for $\cos\theta_W \geq 0.3$ we obtain $\lambda_1^e = -0.092 \pm 0.009$, whereas for $\cos\theta_W \geq 0.8$ we obtain $\lambda_1^e = -0.125 \pm 0.016$.

(2) A larger sample shifts the mean of the λ_1^s distribution closer to zero: the bias induced by the finite sample statistics is smaller, as expected.

The optimal cut on $\cos\theta_W$ is a compromise between having a smaller λ_1^e or having a smaller uncertainty and smaller bias. We estimate the significance of a potential measurement with the figure of merit

$$E = \frac{|\lambda_1^e - \lambda_1^s|}{\sigma_1}, \qquad \sigma_1 = [\sigma_{\lambda_1^e}^2 + (0.1\lambda_1^e)^2]^{\frac{1}{2}}, \tag{31}$$

where in the estimation of the uncertainty σ_1 we have added in quadrature the statistical one and a 10% systematic uncertainty. The numerator $|\lambda_1^e - \lambda_1^s|$ corrects for the bias toward negative values. This simple prescription is sufficient because $|\lambda_1^s|$ is small compared to $|\lambda_1^e|$ and $\sigma_{\lambda_1^e}$, and also the width of the λ_1^s distribution is smaller than $\sigma_{\lambda_1^e}$. The denominator of E takes into account a 10% systematic uncertainty in λ_1^e. For the selected region in (30) we find $E = 7.0$, namely, a significance of 7 standard deviations.

B. tW^- entanglement in the boosted region

For the boosted region, we use the helicity basis. The measurement region is

$$m_{t\bar{t}} \geq 800\ \text{GeV}, \quad |\cos\theta_t| \leq 0.6, \quad \cos\theta_W \leq -0.3. \tag{32}$$

Here we take $\vec{p}_W$ and the top quark momentum $\hat{k}$ in opposite hemispheres, so that the W^- boson is more energetic in the laboratory frame. (This may be an advantage from the experimental point of view.) A completely equivalent analysis can be done with $\cos\theta_W \geq 0.3$. The cross section with these cuts is 197 fb. We assume a luminosity of 139 fb^{-1} with run 2 data and a projection of 250 fb^{-1} at 13.6 TeV in run 3. With these luminosities, the

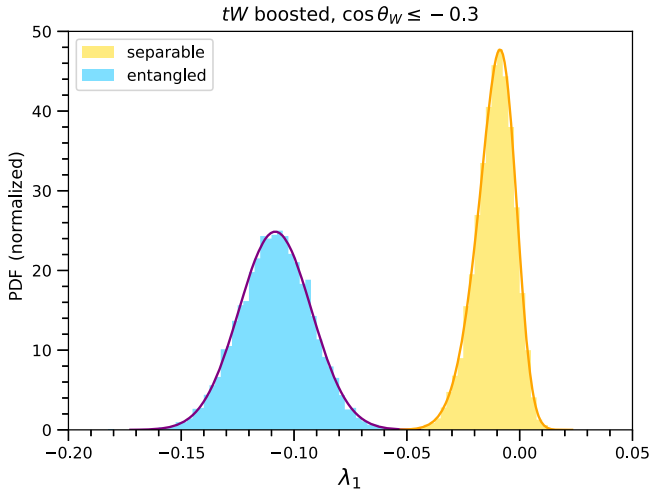

FIG. 2. Probability density functions of (i) λ_1^e in the boosted measurement region (blue), used to determine tW^- entanglement in the SM; and (ii) λ_1^s in its calibration region (yellow), used as a proxy of the lowest eigenvalue for a separable state.

number of expected events is $N = 9800$. The calibration region is $\cos\theta_W \leq -0.9$. The PDFs of λ_1^e and λ_1^s with $n = 10^4$ pseudoexperiments are shown in Fig. 2. The expected sensitivity in the measurement of the lowest eigenvalue of $\rho_{tW}^{T_2}$ is $\lambda_1^e = -0.108 \pm 0.016$. The figure of merit (31) gives a significance of 5.0σ.

C. W^+W^- entanglement near threshold

For completeness, we also study W^+W^- entanglement. We point out that the entanglement between W^+W^- pairs from Higgs boson decays is measurable already with run 2 data [11]. In $t\bar{t}$ decays the distinct feature is the presence of two additional b quarks, which make necessary the use of special kinematical configurations in which the trace over unmeasured b polarizations does not wash out the entanglement.

Because of the limited statistics we only consider a measurement region near threshold,

$$m_{t\bar{t}} \leq 390 \text{ GeV}, \qquad \beta \leq 0.9,$$
$$\cos\theta_{W^+} \geq 0.3, \qquad \cos\theta_{W^-} \leq -0.3, \tag{33}$$

and use the helicity basis. The ranges of $\cos\theta_{W^\pm}$ are chosen to have the $W^\pm$ boson momenta roughly aligned with the parent top (anti)quark momenta in the c.m. frame, so that the $W^\pm$ momenta in the laboratory frame are larger. (There are three additional configurations that give exactly the same significance.) The cross section with the kinematical selection (33) is 600 fb. We assume a luminosity of 139 fb^{-1} with run 2 data, plus 250 fb^{-1} in run 3. With these luminosities, the number of expected events is $N = 29900$. The calibration region is $\cos\theta_{W^+} \geq 0.7$, $\cos\theta_{W^-} \leq -0.7$.

The PDFs of λ_1^e and λ_1^s obtained with $n = 10^4$ pseudoexperiments are presented in Fig. 3. Even if the statistics are comparable to the example in Sec. IV A, the significance is smaller because the central value of the λ_1^e distribution is larger and closer to zero—which is expected because the coherence is partially lost when considering the W^+ boson instead of the top quark. From the pseudoexperiments, we find $\lambda_1^e = -0.0059 \pm 0.004$. The expected significance for the entanglement measurement is 4.0σ.

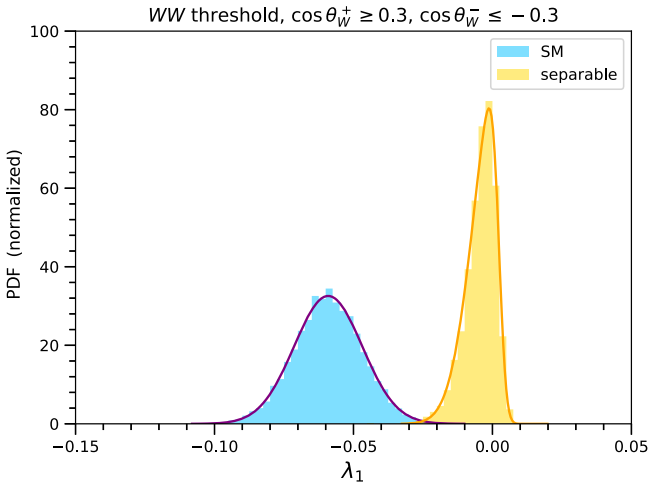

FIG. 3. Probability density functions of (i) λ_1^e in the boosted measurement region (blue), used to determine W^+W^- entanglement in the SM; and (ii) λ_1^s in its calibration region (yellow), used as a proxy of the lowest eigenvalue for a separable state.

V. DISCUSSION

In this work we have addressed the quantum entanglement involving decay products of $t\bar{t}$ pairs produced at the LHC, namely, between the top quark and the W^- boson from the $\bar{t}$ decay (or, equivalently, between $\bar{t}$ and W^+) and between the two W bosons. The key to measure entanglement involving top (anti)quark decay products is to restrict the angle between the W momentum in the parent top rest frame, thereby avoiding the decoherence caused by the sum over the unmeasured b quark polarizations.

We have investigated, with an analysis at the parton level, the feasibility of several measurements. The estimated sensitivities are collected in Table I. For these figures, we have included a bulk reconstruction efficiency of 0.12 and assumed a 10% systematic uncertainty in the entanglement indicator. The sensitivities assuming only statistical uncertainties are also given for reference. We note that several other kinematical regions are possible, which are equivalent from the theoretical point of view and might be more or less favorable experimentally. For WW entanglement, it is also possible that more sensitive tests exist, since the Peres-Horodecki condition is sufficient but not necessary for $\dim\mathcal{H}_A = \dim\mathcal{H}_B = 3$.

A further possibility that could be pursued by experiments to increase the significance is to combine disjoint regions into an entanglement measurement. For example, for tW^- entanglement one could perform two measurements, with $\cos\theta_W \geq 0.3$ and $\cos\theta_W \leq -0.3$, and combine them in order to gain statistics. This type of combination with a proper accounting of systematic uncertainties and correlations can only be performed by an experiment.

In conclusion, $t\bar{t}$ production offers a rare possibility of measuring spin entanglement between a boson and a fermion, which would also constitute the first measurement at the energy frontier, and this would be possible with the data already collected at the LHC run 2.

TABLE I. Summary of expected significance for entanglement measurements.

		Expected significance	
Measurement	Luminosity (fb^{-1})	10% systematics	Statistical only
tW^- threshold	139	7.0σ	9.8σ
tW^- boosted	$139 + 250$	5.0σ	6.1σ
W^+W^- threshold	$139 + 250$	4.0σ	4.5σ

ACKNOWLEDGMENTS

I thank A. Casas and J. Moreno for useful discussions. This work of has been supported by MICINN projects PID2019–110058 GB-C21, PID2022-142545NB-C21, and CEX2020-001007-S funded by MCIN/AEI/10.13039/501100011033, by ERDF, and by Fundação para a Ciência e a Tecnologia (FCT, Portugal) through the project CERN/FIS-PAR/0019/2021.

APPENDIX EXPLICIT EXPRESSIONS FOR *tW* DENSITY OPERATORS

In the basis of the product space $\mathcal{H}_A \otimes \mathcal{H}_B$,

$$\left\{\left|\tfrac{1}{2}\ \ 1\right\rangle,\left|\tfrac{1}{2}\ \ 0\right\rangle,\left|\tfrac{1}{2}\ -1\right\rangle,\left|-\tfrac{1}{2}\ \ 1\right\rangle,\left|-\tfrac{1}{2}\ \ 0\right\rangle,\left|-\tfrac{1}{2}\ -1\right\rangle\right\}, \tag{A1}$$

the matrix elements of the density operator ρ_{tW} are

$$\begin{aligned}
(\rho_{tW})_{11} &= \frac{1}{6}[1+a_0]+\frac{1}{2\sqrt{6}}[A_{10}+C_{010}]+\frac{1}{6\sqrt{2}}[A_{20}+C_{020}],\\
(\rho_{tW})_{12} &= -\frac{1}{2\sqrt{6}}[A_{11}+A_{21}+C_{011}+C_{021}],\\
(\rho_{tW})_{13} &= \frac{1}{2\sqrt{3}}[A_{22}+C_{022}],\\
(\rho_{tW})_{14} &= -\frac{1}{3\sqrt{2}}a_1-\frac{1}{2\sqrt{3}}C_{110}-\frac{1}{6}C_{120},\\
(\rho_{tW})_{15} &= \frac{1}{2\sqrt{3}}[C_{111}+C_{121}],\\
(\rho_{tW})_{16} &= -\frac{1}{\sqrt{6}}C_{122},\\
(\rho_{tW})_{22} &= \frac{1}{6}[1+a_0]-\frac{1}{3\sqrt{2}}[A_{20}+C_{020}],\\
(\rho_{tW})_{23} &= \frac{1}{2\sqrt{6}}[-A_{11}+A_{21}-C_{011}+C_{021}],\\
(\rho_{tW})_{24} &= -\frac{1}{2\sqrt{3}}[C_{11-1}+C_{12-1}],\\
(\rho_{tW})_{25} &= -\frac{1}{3\sqrt{2}}a_1+\frac{1}{3}C_{120},\\
(\rho_{tW})_{26} &= \frac{1}{2\sqrt{3}}[C_{111}-C_{121}],\\
(\rho_{tW})_{33} &= \frac{1}{6}[1+a_0]-\frac{1}{2\sqrt{6}}[A_{10}+C_{010}]\\
&\quad+\frac{1}{6\sqrt{2}}[A_{20}+C_{020}],\\
(\rho_{tW})_{34} &= -\frac{1}{\sqrt{6}}C_{12-2},\\
(\rho_{tW})_{35} &= \frac{1}{2\sqrt{3}}[C_{12-1}-C_{11-1}],\\
(\rho_{tW})_{36} &= -\frac{1}{3\sqrt{2}}a_1+\frac{1}{2\sqrt{3}}C_{110}-\frac{1}{6}C_{120},\\
(\rho_{tW})_{44} &= \frac{1}{6}[1-a_0]+\frac{1}{2\sqrt{6}}[A_{10}-C_{010}]\\
&\quad+\frac{1}{6\sqrt{2}}[A_{20}-C_{020}],\\
(\rho_{tW})_{45} &= \frac{1}{2\sqrt{6}}[-A_{11}-A_{21}+C_{011}+C_{021}],\\
(\rho_{tW})_{46} &= \frac{1}{2\sqrt{3}}[A_{22}-C_{022}],\\
(\rho_{tW})_{55} &= \frac{1}{6}[1-a_0]-\frac{1}{3\sqrt{2}}[A_{20}-C_{020}],\\
(\rho_{tW})_{56} &= \frac{1}{2\sqrt{6}}[-A_{11}+A_{21}+C_{011}-C_{021}],\\
(\rho_{tW})_{66} &= \frac{1}{6}[1-a_0]-\frac{1}{2\sqrt{6}}[A_{10}-C_{010}]\\
&\quad+\frac{1}{6\sqrt{2}}[A_{20}-C_{020}].
\end{aligned} \tag{A2}$$

The operator $\rho_{tW}^{T_2}$ has matrix elements $(\rho_{tW}^{T_2})_{ii}=(\rho_{tW})_{ii}$, $(\rho_{tW}^{T_2})_{jj+3}=(\rho_{tW})_{jj+3}$, for $i=1,\ldots,6$, $j=1,2,3$, and

$$\begin{aligned}
(\rho_{tW}^{T_2})_{12} &= \frac{1}{2\sqrt{6}}[A_{1-1}+A_{2-1}+C_{01-1}+C_{02-1}],\\
(\rho_{tW}^{T_2})_{13} &= \frac{1}{2\sqrt{3}}[A_{2-2}+C_{02-2}],\\
(\rho_{tW}^{T_2})_{15} &= -\frac{1}{2\sqrt{3}}[C_{11-1}+C_{12-1}],\\
(\rho_{tW}^{T_2})_{16} &= -\frac{1}{\sqrt{6}}C_{12-2},\\
(\rho_{tW}^{T_2})_{23} &= \frac{1}{2\sqrt{6}}[A_{1-1}-A_{2-1}+C_{01-1}-C_{02-1}],\\
(\rho_{tW}^{T_2})_{24} &= \frac{1}{2\sqrt{3}}[C_{111}+C_{121}],\\
(\rho_{tW}^{T_2})_{26} &= \frac{1}{2\sqrt{3}}[C_{12-1}-C_{11-1}],\\
(\rho_{tW}^{T_2})_{34} &= -\frac{1}{\sqrt{6}}C_{122},\\
(\rho_{tW}^{T_2})_{35} &= \frac{1}{2\sqrt{3}}[C_{111}-C_{121}],\\
(\rho_{tW}^{T_2})_{45} &= \frac{1}{2\sqrt{6}}[+A_{1-1}+A_{2-1}-C_{01-1}-C_{02-1}],\\
(\rho_{tW}^{T_2})_{46} &= \frac{1}{2\sqrt{3}}[A_{2-2}-C_{02--2}],\\
(\rho_{tW}^{T_2})_{56} &= \frac{1}{2\sqrt{6}}[A_{1-1}-A_{2-1}-C_{01-1}+C_{02-1}].
\end{aligned} \tag{A3}$$

[1] Y. Afik and J. R. M. de Nova, Entanglement and quantum tomography with top quarks at the LHC, Eur. Phys. J. Plus **136**, 907 (2021).

[2] M. Fabbrichesi, R. Floreanini, and G. Panizzo, Testing Bell inequalities at the LHC with top-quark pairs, Phys. Rev. Lett. **127**, 16 (2021).

[3] C. Severi, C. D. Boschi, F. Maltoni, and M. Sioli, Quantum tops at the LHC: From entanglement to Bell inequalities, Eur. Phys. J. C **82**, 285 (2022).

[4] Y. Afik and J. R. M. de Nova, Quantum information with top quarks in QCD, Quantum **6**, 820 (2022).

[5] J. A. Aguilar-Saavedra and J. A. Casas, Improved tests of entanglement and Bell inequalities with LHC tops, Eur. Phys. J. C **82**, 666 (2022).

[6] Y. Afik and J. R. M. de Nova, Quantum discord and steering in top quarks at the LHC, Phys. Rev. Lett. **130**, 221801 (2023).

[7] Z. Dong, D. Gonçalves, K. Kong, and A. Navarro, When the machine chimes the Bell: Entanglement and Bell inequalities with boosted $t\bar{t}$, arXiv:2305.07075.

[8] ATLAS Collaboration, Observation of quantum entanglement in top-quark pair production using pp collisions of $\sqrt{s} = 13$ TeV with the ATLAS detector, Report No. ATLAS-CONF-2023-069.

[9] A. J. Barr, Testing Bell inequalities in Higgs boson decays, Phys. Lett. B **825**, 136866 (2022).

[10] J. A. Aguilar-Saavedra, A. Bernal, J. A. Casas, and J. M. Moreno, Testing entanglement and Bell inequalities in $H \to ZZ$, Phys. Rev. D **107**, 016012 (2023).

[11] J. A. Aguilar-Saavedra, Laboratory-frame tests of quantum entanglement in $H \to WW$, Phys. Rev. D **107**, 076016 (2023).

[12] R. Ashby-Pickering, A. J. Barr, and A. Wierzchucka, Quantum state tomography, entanglement detection and Bell violation prospects in weak decays of massive particles, J. High Energy Phys. 05 (2023) 020.

[13] M. Fabbrichesi, R. Floreanini, E. Gabrielli, and L. Marzola, Bell inequalities and quantum entanglement in weak gauge bosons production at the LHC and future colliders, Eur. Phys. J. C **83**, 823 (2023).

[14] R. A. Morales, Exploring Bell inequalities and quantum entanglement in vector boson scattering, arXiv:2306.17247.

[15] M. M. Altakach, P. Lamba, F. Maltoni, K. Mawatari, and K. Sakurai, Quantum information and CP measurement in $H \to \tau^+\tau^-$ at future lepton colliders, Phys. Rev. D **107**, 093002 (2023).

[16] A. Feist, G. Huang, G. Arend, Y. Yang, J. W. Henke, A. S. Raja, F. J. Kappert, R. N. Wang, H. Lourenço-Martins, Z. Qiu *et al.*, Cavity-mediated electron-photon pairs, Science **377**, 777 (2022).

[17] A. Peres, Separability criterion for density matrices, Phys. Rev. Lett. **77**, 1413 (1996).

[18] P. Horodecki, Separability criterion and inseparable mixed states with positive partial transposition, Phys. Lett. A **232**, 333 (1997).

[19] J. A. Aguilar-Saavedra and J. Bernabeu, Breaking down the entire W boson spin observables from its decay, Phys. Rev. D **93**, 011301 (2016).

[20] J. A. Aguilar-Saavedra, Crafting polarizations for top, W, and Z, Phys. Rev. D **106**, 115021 (2022).

[21] R. Rahaman and R. K. Singh, Breaking down the entire spectrum of spin correlations of a pair of particles involving fermions and gauge bosons, Nucl. Phys. **B984**, 115984 (2022).

[22] J. Alwall, R. Frederix, S. Frixione, V. Hirschi, F. Maltoni, O. Mattelaer, H. S. Shao, T. Stelzer, P. Torrielli, and M. Zaro, The automated computation of tree-level and next-to-leading order differential cross sections, and their matching to parton shower simulations, J. High Energy Phys. 07 (2014) 079.

[23] R. D. Ball *et al.* (NNPDF Collaboration), Parton distributions from high-precision collider data, Eur. Phys. J. C **77**, 663 (2017).

[24] W. Bernreuther, A. Brandenburg, Z. G. Si, and P. Uwer, Top quark spin correlations at hadron colliders: Predictions at next-to-leading order QCD, Phys. Rev. Lett. **87**, 242002 (2001).

[25] A. Brandenburg, Z. G. Si, and P. Uwer, QCD corrected spin analyzing power of jets in decays of polarized top quarks, Phys. Lett. B **539**, 235 (2002).

[26] M. Czakon and A. Mitov, Top++: A program for the calculation of the top-pair cross-section at hadron colliders, Comput. Phys. Commun. **185**, 2930 (2014).

[27] M. Aaboud *et al.* (ATLAS Collaboration), Measurements of top quark spin observables in $t\bar{t}$ events using dilepton final states in $\sqrt{s} = 8$ TeV pp collisions with the ATLAS detector, J. High Energy Phys. 03 (2017) 113.

[28] A. M. Sirunyan *et al.* (CMS Collaboration), Measurement of the top quark polarization and $t\bar{t}$ spin correlations using dilepton final states in proton-proton collisions at $\sqrt{s} = 13$ TeV, Phys. Rev. D **100**, 072002 (2019).

[29] B. Abbott *et al.* (D0 Collaboration), Measurement of the top quark mass using dilepton events, Phys. Rev. Lett. **80**, 2063 (1998).

[30] V. Khachatryan *et al.* (CMS Collaboration), Measurement of the differential cross section for top quark pair production in pp collisions at $\sqrt{s} = 8$ TeV, Eur. Phys. J. C **75**, 542 (2015).

[31] J. A. Aguilar-Saavedra, M. C. N. Fiolhais, P. Martín-Ramiro, J. M. Moreno, and A. Onofre, A template method to measure the $t\bar{t}$ polarisation, Eur. Phys. J. C **82**, 134 (2022).

[32] G. Aad *et al.* (ATLAS Collaboration), Measurement of the top quark pair production charge asymmetry in proton-proton collisions at $\sqrt{s} = 7$ TeV using the ATLAS detector, J. High Energy Phys. 02 (2014) 107.

[33] W. Bernreuther, D. Heisler, and Z. G. Si, A set of top quark spin correlation and polarization observables for the LHC: Standard model predictions and new physics contributions, J. High Energy Phys. 12 (2015) 026.